Zn^{2+} current is mediated by voltage-gated Ca^{2+} channels and enhanced by extracellular acidity in mouse cortical neurones

Geoffrey A. Kerchner, Lorella M. T. Canzoniero, Shan Ping Yu, Cliff Ling* and Dennis W. Choi

*Center for the Study of Nervous System Injury and Department of Neurology, Washington University School of Medicine, 660 S. Euclid Avenue, St Louis, MO 63110 and *Analytical Sciences Center, Monsanto Company, 800 N. Lindbergh Boulevard, St Louis, MO 63167, USA*

(Received 30 March 2000; accepted after revision 8 June 2000)

1. Mammalian neuronal voltage-gated Ca^{2+} channels have been implicated as potential mediators of membrane permeability to Zn^{2+}. We tested directly whether voltage-gated Ca^{2+} channels can flux Zn^{2+} in whole-cell voltage-clamp recordings from cultured murine cortical neurones.

2. In the presence of extracellular Zn^{2+} and no Na^+, K^+, or other divalent cations, a small, non-inactivating, voltage-gated inward current was observed exhibiting a current–voltage relationship characteristic of high-voltage activated (HVA) Ca^{2+} channels. Inward current was detectable at Zn^{2+} levels as low as 50 μM, and both the amplitude and voltage sensitivity of the current depended upon Zn^{2+} concentration. This Zn^{2+} current was sensitive to blockade by Gd^{3+} and nimodipine and, to a lesser extent, by ω-conotoxin GVIA.

3. Zn^{2+} could permeate Ca^{2+} channels in the presence of Ca^{2+} and other physiological cations. Inward currents recorded with 2 mM Ca^{2+} were attenuated by Zn^{2+} ($IC_{50} = 210$ μM), and currents recorded with Zn^{2+} were unaffected by up to equimolar Ca^{2+} concentrations. Furthermore, the Zn^{2+}-selective fluorescent dye Newport Green revealed a depolarisation-activated, nimodipine-sensitive Zn^{2+} influx into cortical neurones that were bathed in a physiological extracellular solution plus 300 μM $ZnCl_2$.

4. Surprisingly, while lowering extracellular pH suppressed HVA Ca^{2+} currents, Zn^{2+} current amplitude was affected oppositely, varying inversely with pH with an apparent pK of 7·4. The acidity-induced enhancement of Zn^{2+} current was associated with a positive shift in reversal potential but no change in the kinetics or voltage sensitivity of channel activation.

5. These results provide evidence that L- and N-type voltage-gated Ca^{2+} channels can mediate Zn^{2+} entry into cortical neurones and that this entry may be enhanced by extracellular acidity.

Zinc is concentrated in the synaptic vesicles of central excitatory nerve terminals (Perez-Clausell & Danscher, 1985) and is released upon synaptic activation (Assaf & Chung, 1984; Howell *et al.* 1984). The total concentration of Zn^{2+} in the hippocampus and cortical grey matter has been estimated at 220–300 μM (Frederickson, 1989), and peak concentrations of synaptically released Zn^{2+} may reach hundreds of micromolar in hippocampal slices (Assaf & Chung, 1984; Vogt *et al.* 2000) – concentrations more than sufficient for Zn^{2+} to exhibit profound modulatory effects on a variety of agonist- and voltage-gated mammalian ion channels, including attenuation of current through NMDA and GABA receptor-gated channels, potentiation of AMPA, glycine, and ATP receptor-mediated currents, modulation of the transient outward K^+ current I_A, and blockade of voltage-gated Na^+ and Ca^{2+} channels (Harrison & Gibbons, 1994; Smart *et al.* 1994).

Excessive exposure to extracellular Zn^{2+} can also be toxic to neurones (Yokoyama *et al.* 1986), inducing apoptosis at lower concentrations (Manev *et al.* 1997; Lobner *et al.* 2000) and necrosis at higher concentrations (Choi *et al.* 1988; Lobner *et al.* 2000). Zn^{2+} neurotoxicity has been implicated in the pathogenesis of selective neuronal death following transient global cerebral ischaemia and prolonged seizures (Choi & Koh, 1998). A critical step in Zn^{2+}-induced neuronal death appears to be its permeation across the plasma membrane (Tønder *et al.* 1990; Weiss *et al.* 1993; Koh *et al.* 1996). Raising extracellular Ca^{2+} reduces Zn^{2+} neurotoxicity

(Weiss *et al.* 1993; Koh & Choi, 1994), suggesting that routes implicated in membrane permeability to Ca^{2+} may also mediate Zn^{2+} flux (Choi & Koh, 1998). Putative routes of neuronal Zn^{2+} entry include Ca^{2+}-permeable AMPA (Yin & Weiss, 1995; Sensi *et al.* 1997) and NMDA (Christine & Choi, 1990; Koh & Choi, 1994) receptor-gated channels, as well as transporter-mediated exchange with intracellular Na^+ (Sensi *et al.* 1997). An especially prominent route of toxic Zn^{2+} entry may be voltage-gated Ca^{2+} channels, as neuronal depolarisation enhanced both Zn^{2+} influx and resultant neuronal death, and Ca^{2+} channel antagonists attenuated both indices (Weiss *et al.* 1993; Freund & Reddig, 1994; Manev *et al.* 1997).

Zn^{2+} is a potent antagonist of voltage-gated Ca^{2+} channels in invertebrates (Hagiwara & Takahashi, 1967) and mammals (Winegar & Lansman, 1990; Büsselberg *et al.* 1992). There is also clear evidence that Zn^{2+} can permeate voltage-gated Ca^{2+} channels in invertebrates: in the absence of Ca^{2+}, Zn^{2+} can support full Ca^{2+} channel-mediated action potentials in insect muscle membranes (Fukuda & Kawa, 1977) and snail neurones (Kawa, 1979). In addition, nanoampere-sized whole-cell Zn^{2+} currents through verapamil- and Co^{2+}-sensitive channels have been characterised in *Helix* neurones (Oyama *et al.* 1982). However, the evidence for Zn^{2+} permeation of voltage-gated Ca^{2+} channels in mammals has so far been only indirect. Voltage-gated Ca^{2+} channel antagonists, including dihydropyridine compounds and ω-conotoxin GVIA in particular, attenuated depolarisation-induced intracellular Zn^{2+} accumulation as measured by transcription of a reporter gene coupled to a Zn^{2+}-activated metallothionein promoter in pituitary tumour cells (Atar *et al.* 1995), fluorescence of a Zn^{2+}-sensitive dye loaded into living cortical neurones (Sensi *et al.* 1997), and cortical neuronal uptake of $^{65}Zn^{2+}$ (H. Ying and D. W. Choi, unpublished observations), suggesting that Zn^{2+} may permeate L- and N-type HVA Ca^{2+} channels. Although two reports exist of small (< 50 pA) inward whole-cell currents recorded in the presence of extracellular Zn^{2+} in bovine chromaffin cells (Vega *et al.* 1994) and rat ventricular myocytes (Atar *et al.* 1995), neither study directly implicated Zn^{2+} as the charge carrier or provided any characterisation of the currents observed. In this study, we sought to test whether cortical neuronal voltage-gated Ca^{2+} channels flux Zn^{2+}. We showed that Zn^{2+} could indeed permeate these channels and, in addition, that it could do so in the ionic conditions normally encountered in the brain. Furthermore, we have demonstrated that extracellular acidity enhanced the permeation of Zn^{2+} relative to Ca^{2+} through voltage-gated Ca^{2+} channels. An abstract based on these results has appeared (Kerchner *et al.* 1998).

METHODS

Murine cortical cell cultures

Mixed cortical cultures, containing both neurones and glia, were prepared from embryonic day 15 mice as described previously (Rose *et al.* 1993). Embryos were harvested acutely from pregnant female mice killed under halothane anaesthesia by cervical dislocation. Embryos were decapitated, and neocortices were dissected, dissociated, and plated in Eagle's minimal essential medium (MEM, Earle's salts) supplemented with 20 mM glucose (final concentration 25 mM), 2 mM glutamine, 5% fetal bovine serum, and 5% horse serum at a density of 0·4 hemispheres per dish onto 35 mm culture dishes (Becton Dickinson and Company, Plymouth, UK), which were prepared by incubation overnight with 1 mg ml^{-1} poly-D-lysine (Sigma Chemical Co.) and 20 μg ml^{-1} laminin (Collaborative Biomedical Products, Bedford, MA, USA) and subsequent rinsing with water. The medium was changed after 9 days *in vitro* (DIV 9) to MEM containing 25 mM glucose and 2 mM glutamine. Cultures were maintained in a 37 °C, humidified incubator in a 5% CO_2 atmosphere. All experiments were performed between DIV 14 and 17. Protocols for the handling of experimental animals were approved by the Animal Studies Committee at Washington University School of Medicine, in accordance with local and national ethical guidelines.

Electrophysiology

Whole-cell voltage-clamp recordings were performed on cultured murine cortical neurones in 35 mm dishes on the stage of an inverted microscope (Nikon, Japan) using an Axopatch 200A amplifier (Axon Instruments Inc.). Patch electrodes were pulled from borosilicate glass capillary tubes (World Precision Instruments) using a Flaming-Brown micropipette puller (Sutter Instrument Co.) and fire polished to a final tip resistance of 7–12 MΩ when filled with the internal pipette solution (Table 1). Capacitance neutralisation and series resistance compensation were routinely applied, and input resistance was typically ~400–500 MΩ in the standard external solution (Table 1). Current was digitally sampled at 20 kHz and filtered by a 5 kHz, 4-pole low-pass Bessel filter. Current traces were displayed and stored on an IBM PC-compatible computer (Comtrade Express) using the A/D converter interface Digidata 1200 and the data acquisition/analysis software package pCLAMP 6.0 (Axon Instruments Inc.). Leak subtraction was performed by pCLAMP by delivering two negative-going voltage pulses, each half the height of the test pulse, from a holding potential of −90 mV, before delivery of each depolarising test pulse from −70 mV. All experiments were performed at room temperature (21–22 °C). Data are reported as means ± standard error of the mean (S.E.M.).

Solution preparation and delivery

The contents of the standard external bath and internal pipette solutions are itemised in Table 1. To aid in the formation of a tight electrical seal between the glass pipette and the neuronal membrane, cells were initially bathed in standard external solution supplemented with 2 mM $MgCl_2$. During recordings, a neurone was bathed in a control solution with no divalent cations, one supplemented with $CaCl_2$ or $ZnCl_2$, or one supplemented both with $ZnCl_2$ and a pharmacological agent. In each case, solutions were delivered directly to the tested neurone by continuous perfusion with a gravity-fed delivery pipette of approximately 300 μm internal diameter. Solution changes occurred at a cell in less than 100 ms.

Current–voltage curve fits

In Figs 4 and 9, current–voltage relations were fitted with curves to allow determination and comparison of the voltage sensitivity of channel activation in different conditions. At some voltage V:

$$I = -P_o(V_{rev} - V)g,$$

where I is the magnitude of current measured in relative units, P_o is the proportion of channels open at V, V_{rev} is the reversal potential of the current, and g is proportional to membrane conductance

when channels are fully activated. P_o is described by the Boltzmann relation:

$$P_o = \frac{1}{1 + \exp[(V_h - V)/m]},$$

where V_h is the voltage of half-maximal channel activation, and m is a slope factor. These equations apply whether I represents the contribution of a single ion (e.g. Zn^{2+}) flowing into a cell or the net current resulting from multiple conductances (e.g. Zn^{2+} flowing into and Na^+ flowing out of a cell); in the latter case, g would represent the sum of conductances, and V_{rev} would represent the net reversal potential of the current, an average of the V_{rev} values for each ion weighted by the relative contribution of each ion's conductance to the total membrane conductance. Curves were fitted by least-squares regression.

Fluorescence detection of intracellular Zn^{2+}

The intracellular Zn^{2+} concentration ($[Zn^{2+}]_i$) was assessed using Newport Green as previously described (Canzoniero *et al.* 1999). Cell cultures were first washed with a Hepes-buffered physiological saline solution containing (mM): NaCl 120, KCl 5·4, $MgCl_2$ 0·8, Hepes 20, glucose 15, $CaCl_2$ 1·8, NaOH 10 (pH 7·4). Cells were then loaded with 5 μM Newport Green diacetate (excitation wavelength (λ), 485 nm; emission λ, 530 nm; Molecular Probes) in the presence of 0·02% Pluronic F-127 for 30 min at room temperature. Neurones were washed and incubated for an additional 30 min in the Hepes-buffered saline. Before each experiment, cultures were washed twice with the same solution.

All experiments were performed at room temperature under constant perfusion (2 ml min^{-1}) on the stage of a Nikon Diaphot inverted microscope equipped with a 75 W xenon lamp and a Nikon ×40, 1·3 NA epifluorescence oil immersion objective lens. Background fluorescence was subtracted at the beginning of each experiment. Images were acquired with a CCD camera (Quantex, CA, USA) and digitised using Metafluor 4.0 software (Universal Imaging, West Chester, PA, USA).

$[Zn^{2+}]_i$ was calculated using *in situ* calibration at the end of each experiment. For each field of neurones, maximum (F_{max}) and minimum (F_{min}) fluorescence values were determined by exposure to 1 mM Zn^{2+}plus 50 μM sodium pyrithione or to the heavy metal chelator *N,N,N′,N′*-tetrakis(2-pyridylmethyl)ethylenediamine (TPEN, 100 μM) in a Zn^{2+}-, Mg^{2+}- and Ca^{2+}-free medium, respectively. An assumed K_d of 1 μM (Haugland, 1996) was applied to the formula described by Grynkiewicz *et al.* (1985), which gives that for a fluorescence value F:

$$[Zn^{2+}]_i = K_d[(F - F_{min})/(F_{max} - F)].$$

The experiments were performed twice with similar results.

Atomic zinc analysis

Samples (prepared according to Table 3) were transferred to a quartz beaker and treated with concentrated sulphuric acid. A sample was then repeatedly charred on a hot plate at 250 °C and treated with nitric acid until the sample no longer charred, at which point the sample was resuspended in doubly deionised water. A determination of the zinc content of these samples was performed with an inductively-coupled plasma atomic emission spectrometer, the Thermo Jarrell Ash IRIS Advantage Duo-View System (Thermo Jarrell Ash Corp., Franklin, MA, USA).

Chemicals and pharmacological agents

All chemicals were purchased from Sigma Chemical Co. except ω-conotoxin GVIA which was from Bachem Biosciences Inc. (King of Prussia, PA, USA).

Table 1. Composition of electrophysiological recording solutions (concentrations in mM except as indicated)

Solute	Internal (all expts)	External	
		Expts at constant pH	Expts at varying pH
NMDG	—	122	120
$ZnCl_2$ or $CaCl_2$	—	As indicated	As indicated
TEA-Cl	130	20	20
Hepes	10	5	—
Hepes or Pipes	—	—	10
Glucose	—	10	10
$MgCl_2$	3	—	—
BAPTA	2·5	—	—
Na_2-ATP	5	—	—
Li-GTP	0·3	—	—
TTX	—	200 nM	200 nM
HCl	—	To pH 7·4	To indicated pH
TEA-OH	To pH 7·4	—	—

Abbreviations: NMDG, *N*-methyl-D-glucamine; TEA-Cl, tetraethylammonium chloride; Hepes, *N*-(2-hydroxyethyl)piperazine-*N′*-(2-ethanesulfonic acid); Pipes, piperazine-*N,N′*-bis(2-ethanesulfonic acid); BAPTA, 1,2-bis(2-aminophenoxy)-ethane-*N,N,N′,N′*-tetraacetic acid; TTX, tetrodotoxin.

RESULTS

A voltage-gated current is observed in the presence of Zn^{2+}

When extracellular Ca^{2+} is lowered below micromolar levels, voltage-gated Ca^{2+} channels become highly permeable to other divalent and monovalent ions including Na^+ and K^+ (Kostyuk *et al.* 1983; Almers & McCleskey, 1984). To isolate any Zn^{2+} permeation through voltage-gated Ca^{2+} channels, voltage-clamp recordings of cultured cortical neurones were made using an internal solution containing TEA to block voltage-gated K^+ channels and an external solution nominally devoid of any divalent cations, Na^+ and K^+ (Table 1) to eliminate contributions of these ions to inward whole-cell currents. Under these conditions, no membrane current was observed during a voltage step from −70 to +10 mV, whereas in the presence of 2 mM extracellular Zn^{2+}, a sustained inward current appeared (Fig. 1*A*) with an average steady-state amplitude of -19 ± 1 pA ($n = 33$) and a current–voltage (I–V) relationship consistent with mediation by voltage-gated Ca^{2+} channels (Fig. 1*B*). No significant voltage-dependent steady-state inactivation was observed in inward currents recorded in the presence of Zn^{2+} after prepulses of 1 s duration, although currents carried by Ca^{2+} showed substantial inactivation in the same conditions (Fig. 2). To compare the activation kinetics of inward currents recorded in the presence of either Zn^{2+} or Ca^{2+}, the 10–90% rise times of currents elicited by voltage steps to 0 mV were measured, revealing a slower activation phase when Zn^{2+} rather than Ca^{2+} was used as the putative charge carrier (Table 2).

Table 2. Rise times of currents carried by Zn^{2+} or Ca^{2+}

Charge carrier	pH	10–90 % rise time (ms)	n
Ca^{2+} (1 mM)	7·4	5·5 ± 0·5	7
Zn^{2+} (0·5 mM)	7·4	12 ± 2	12
Zn^{2+} (0·5 mM)	6·4	14 ± 2	12

Rise times were calculated from the rising phase of currents evoked by voltage steps from −70 to 0 mV. Rise times differ significantly between Zn^{2+} and Ca^{2+} currents at pH 7·4 ($P < 0·05$, Student's t test) but not between Zn^{2+} currents at pH 7·4 and 6·4.

Zn^{2+} concentration affects current amplitude and voltage sensitivity

To test the hypothesis that Zn^{2+} was the charge carrier for the inward current described above, the effects of varying the extracellular Zn^{2+} concentration ($[Zn^{2+}]_o$) were explored. As $[Zn^{2+}]_o$ was increased through a range from 200 μM to 1 mM, the steady-state inward current amplitudes elicited by voltage steps from −70 to 0 mV increased (Fig. 3). Increasing $[Zn^{2+}]_o$ to 2 mM did not increase inward current amplitude any further.

To determine whether this positive correlation between $[Zn^{2+}]_o$ and steady-state current amplitude at 0 mV was due to an increase in maximum steady-state current amplitude

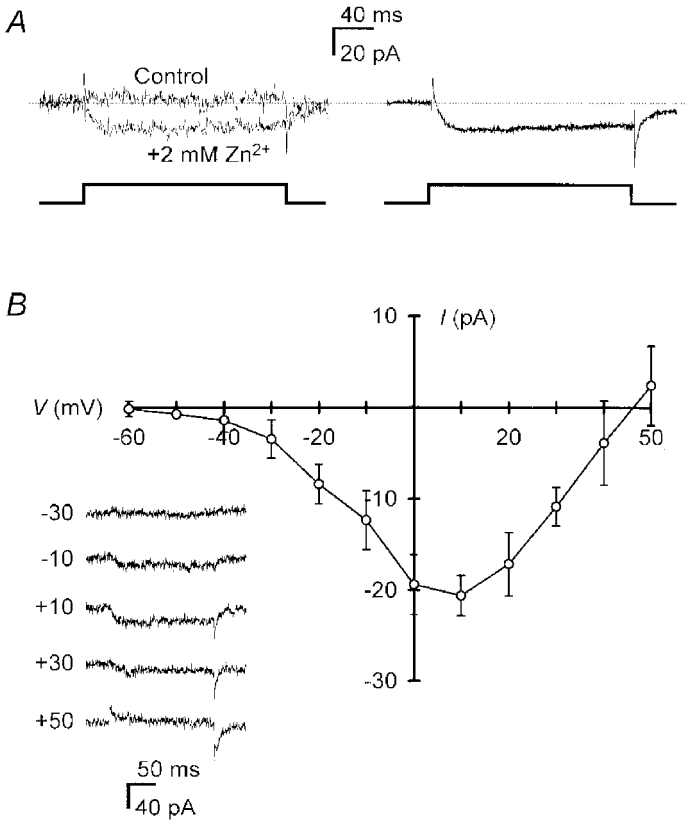

Figure 1. Zn^{2+} produced an inward current in cultured cortical neurones

A, an inward current was elicited in the presence but not the absence (Control) of 2 mM Zn^{2+} by a voltage step to +10 mV. Illustrated are superimposed traces from a representative cell (left; data filtered at 0·5 kHz for display) and the averaged current from 33 cells in 2 mM Zn^{2+} (right; no additional filter). Dotted line indicates the baseline zero current level for these leak-subtracted traces (see Methods). *B*, the *I–V* relationship of steady-state current recorded during voltage steps from −70 mV in the presence of 2 mM Zn^{2+} is shown as the mean ± S.E.M. of 5 cells. Sample traces over a range of voltages (mV) are illustrated for a representative cell (inset; current traces here and in subsequent figures were filtered at 1 or 2 kHz to optimise legibility). 'Steady-state current' in these and the other experiments reported here refers to an average of the sustained component of current, minus baseline, during a voltage step; for instance, the average current recorded during the last 100 ms of a 200 ms pulse. A reversal potential appears in this *I–V* relationship, and an outward current was evident at positive potentials. This outward current was probably not carried by Zn^{2+} that had accumulated within a cell during experiments, as recorded cells were perfused with BAPTA (2 mM; K_d for $Zn^{2+} = 1–10$ nM; Aballay *et al.* 1995). More likely, intracellular cations such as Na^+ and Li^+ (Table 1), as well as some residual K^+, may have accounted for the outward conductance, by analogy with the known effect of intracellular monovalent cations to influence the experimentally observed reversal potential of voltage-gated Ca^{2+} currents (Hille, 1992).

or a shift in the *I–V* relationship, *I–V* curves were constructed in the presence of 50 μM and 2 mM extracellular Zn^{2+} (Fig. 4*A*). The maximum steady-state current amplitude recorded in the presence of 2 mM Zn^{2+} was larger than in 50 μM Zn^{2+}. In addition, the *I–V* curve peak in 2 mM Zn^{2+} occurred at a more depolarised membrane potential than in 50 μM Zn^{2+}. When curves were fitted to the *I–V* data, the voltage dependence of channel activation could be approximated (see Methods). Raising the Zn^{2+} concentration caused the channel activation–voltage relationship to shift rightwards with some reduction in slope; V_h was approximately −22 mV in 50 μM Zn^{2+} and +2·1 mV in 2 mM Zn^{2+} (Fig. 4*B*).

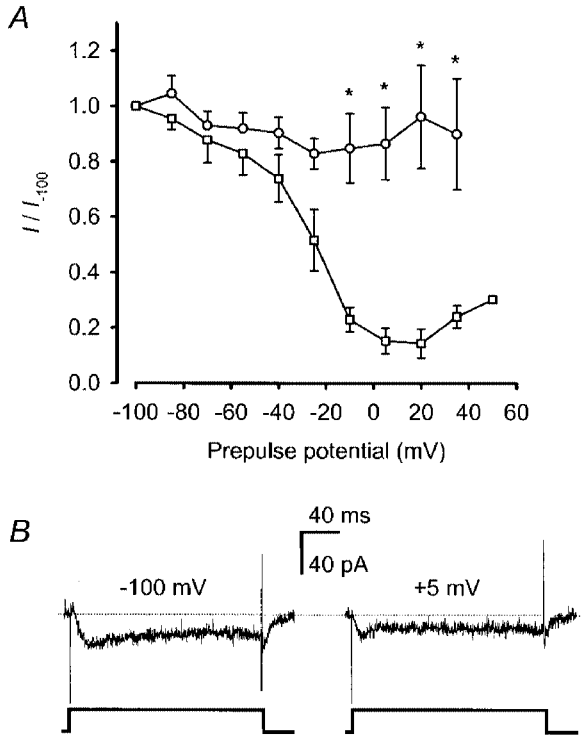

Figure 2. Zn^{2+} current exhibited no voltage-dependent steady-state inactivation

A, after 1 s prepulses to the indicated potentials, the amplitude of steady-state inward currents elicited by immediately subsequent voltage steps to 0 mV in the presence of 500 μM Zn^{2+} (○; $n = 6$) or 2 mM Ca^{2+} (□; $n = 3$) are plotted relative to values obtained after a prepulse to −100 mV. In each cell tested, families of voltage pulses were delivered twice – once in an ascending order (−100 to +50 mV), and once in a descending order, to help compensate for any non-voltage-dependent current run-down. * Significant difference between relative current amplitudes recorded in Zn^{2+} *versus* Ca^{2+} after the indicated prepulse potentials (two-way ANOVA with Bonferroni's *t* test). Points represent means ± S.E.M. *B*, traces obtained by voltage steps from −70 to 0 mV after a 1 s prepulse to −100 mV (left) or +5 mV (right) are illustrated for the cell for which the greatest degree of inactivation was observed in the presence of 500 μM Zn^{2+}. The dotted line indicates the zero current level. The sustained component (latter 100 ms) of the inward currents were compared to generate the graph in *A*.

Zn^{2+} current is blocked by voltage-gated Ca^{2+} channel antagonists

To investigate whether voltage-gated Ca^{2+} channels mediated the inward current recorded in the presence of 2 mM Zn^{2+} and to determine which subtypes of these channels were involved, we tested voltage-gated Ca^{2+} channel antagonists for their effects on the current (Fig. 5*A*). Gd^{3+} (10 μM), a non-subtype-selective Ca^{2+} channel antagonist (Lansman, 1990; Canzoniero *et al.* 1993), suppressed steady-state current amplitude by 86 ± 5% ($n = 8$). Nimodipine (1 μM), an L-type Ca^{2+} channel antagonist, attenuated a larger portion of the inward current (81 ± 10%; $n = 6$) than ω-conotoxin GVIA (1 μM; 33 ± 4%; $n = 6$), an N-type Ca^{2+} channel antagonist. In contrast, MK-801 (1 μM), an NMDA receptor-gated channel blocker, had no effect on the current amplitude (0·0 ± 8% compared to controls; $n = 3$). Further experiments with nimodipine demonstrated that its inhibition of a Zn^{2+} current was reversible (Fig. 5*B*) and occurred at all voltage levels (Fig. 5*C*).

Voltage-gated Ca^{2+} channel-mediated Zn^{2+} influx can occur in the presence of Ca^{2+}

While isolating the contribution of Zn^{2+} to voltage-gated inward currents required the removal of other mono- and divalent cations – including Ca^{2+}, in particular – from the extracellular bathing solution, it is important to determine whether voltage-gated Ca^{2+} channel-mediated Zn^{2+} entry can occur in physiological solutions. First, the effect of extracellular Ca^{2+} on Zn^{2+} current was examined. When inward currents were generated by voltage steps in the presence of 2 mM Zn^{2+}, extracellular Ca^{2+} up to 2 mM had no effect on steady-state current amplitude ($n = 7$–14 cells per Ca^{2+} concentration; Fig. 6*A*). At 10 mM Ca^{2+}, the net amplitude of inward current doubled compared to the level

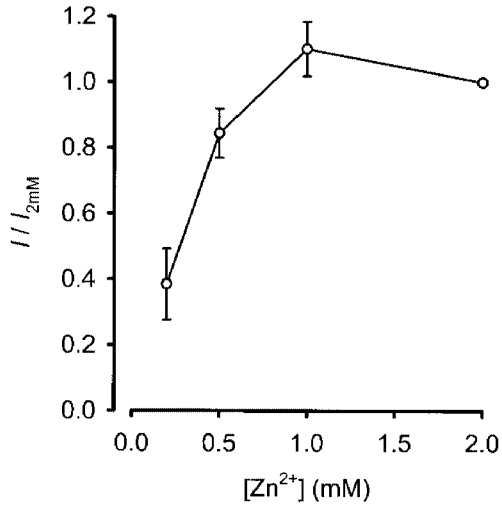

Figure 3. Inward current amplitude at 0 mV depended upon extracellular Zn^{2+} concentration

Increasing $[Zn^{2+}]_o$ increased the amplitude of steady-state currents elicited by voltage steps to 0 mV. Points represent means ± S.E.M. of 4–7 cells and are plotted relative to currents elicited in the presence of 2 mM Zn^{2+}.

of current recorded in Zn^{2+} alone, but it was not as high as the currents measured in the presence of 2 mM Ca^{2+} alone ($n = 4$; Fig. 6*A*), suggesting that the presence of Zn^{2+} impeded Ca^{2+} permeation. To confirm that Zn^{2+} could block cortical neuronal voltage-gated Ca^{2+} current as reported previously in other systems (see Introduction), the effect of Zn^{2+} on voltage-gated inward currents generated in the presence of 2 mM Ca^{2+} was tested. In contrast to the effect of Ca^{2+} on Zn^{2+} current, Zn^{2+} exerted a dose-dependent depression of Ca^{2+} current, with an approximate IC_{50} of 210 μM ($n = 4$; Fig. 6*B*).

Since it is impossible to assign to Zn^{2+} a defined portion of the inward current evoked in the presence of extracellular Ca^{2+} plus Zn^{2+}, we turned to Zn^{2+}-selective fluorimetric imaging to verify that Zn^{2+} can permeate voltage-gated Ca^{2+} channels in the presence of physiological extracellular cation concentrations. Cortical neurones were loaded with the Zn^{2+}-selective fluorescent probe Newport Green, which is capable of discriminating Zn^{2+} from other divalent cations, including Ca^{2+} and Mg^{2+} (Canzoniero *et al.* 1999; Sensi *et al.* 1999). When Newport Green-loaded neurones were exposed to depolarising conditions (60 mM KCl, 2 min)

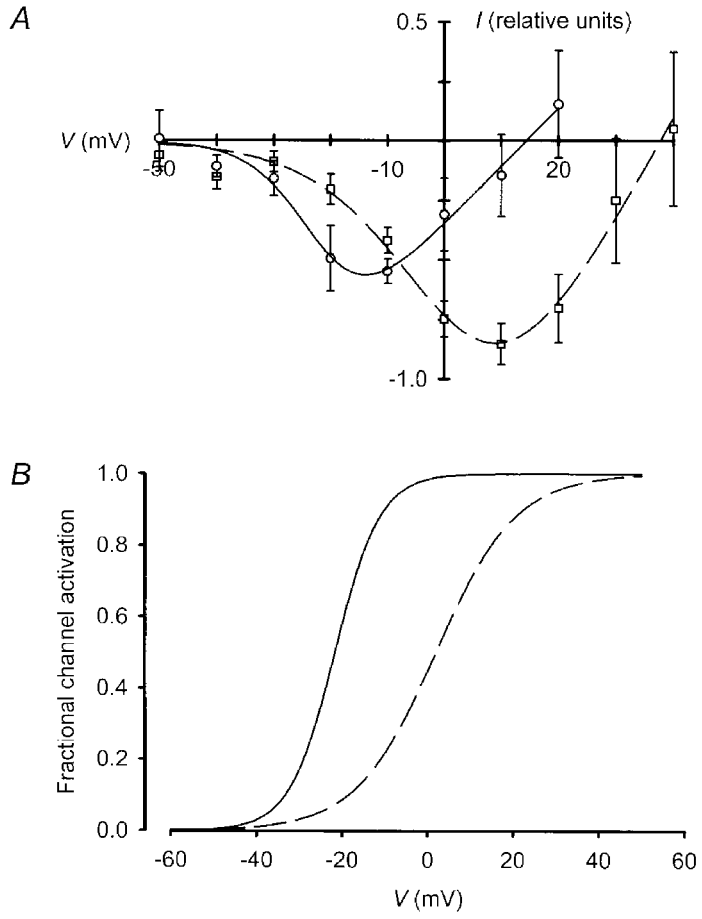

Figure 4. Zn^{2+} concentration affected both maximal current amplitude and voltage sensitivity
A, increasing $[Zn^{2+}]_o$ from 50 μM (○—○) to 2 mM (□– –□) resulted in both an increased maximum steady-state current amplitude ($P < 0{\cdot}05$, Student's paired t test comparing I–V curve peaks in 50 μM and 2 mM Zn^{2+}), and a rightward shift of the I–V relationship. Five cells were tested, each at both Zn^{2+} concentrations to maximise comparability of the data, and I–V curves for each cell were normalised to the peak steady-state inward current in 2 mM Zn^{2+}. As each cell was first tested in 50 μM Zn^{2+} and then in 2 mM Zn^{2+}, some current run-down is the likely explanation for why the current at 0 mV in 2 mM Zn^{2+} was not as much larger than the current in 50 μM Zn^{2+} as would be predicted from the data in Fig. 3. Points represent means ± S.E.M. Curves fitted to the points are described by the equation:

$$I_{\text{relative}} = -\{1 + \exp[(V_h - V)m^{-1}]\}^{-1} \times (V_{\text{rev}} - V)g$$

(see Methods). In 2 mM Zn^{2+}, $V_h = 2{\cdot}1$ mV, $m = 9{\cdot}4$, $V_{\text{rev}} = 38$ mV, and $g = 0{\cdot}044$; in 50 μM Zn^{2+}, $V_h = -22$ mV, $m = 5{\cdot}3$, $V_{\text{rev}} = 14$ mV, and $g = 0{\cdot}025$. *B*, increasing $[Zn^{2+}]_o$ from 50 μM (continuous line) to 2 mM (dashed line) resulted in a shift of the voltage sensitivity of channel activation to more depolarised potentials. Boltzmann curves, described by the equation $I_{\text{relative}} = \{1 + \exp[(V_h - V)m^{-1}]\}^{-1}$, are plotted using values for V_h and m derived from curve fits to the I–V data (*A*) to ease comparison of those two variables between conditions.

in the presence of physiological extracellular cation concentrations plus 300 μM Zn^{2+}, a marked increase in $[Zn^{2+}]_i$ was detected. The addition of nimodipine (10 μM) substantially attenuated the KCl-induced $[Zn^{2+}]_i$ increase, confirming that Zn^{2+} entry occurred predominantly through L-type Ca^{2+} channels (Fig. 7).

Zn^{2+} current is enhanced by extracellular acidity

Lowering extracellular pH (pH_o) suppresses HVA Ca^{2+} channel currents carried by Ca^{2+}, Ba^{2+}, or monovalent cations in a variety of cell types including hippocampal neurones (e.g. Tombaugh & Somjen, 1996), and we examined the effect of this manoeuvre on inward currents

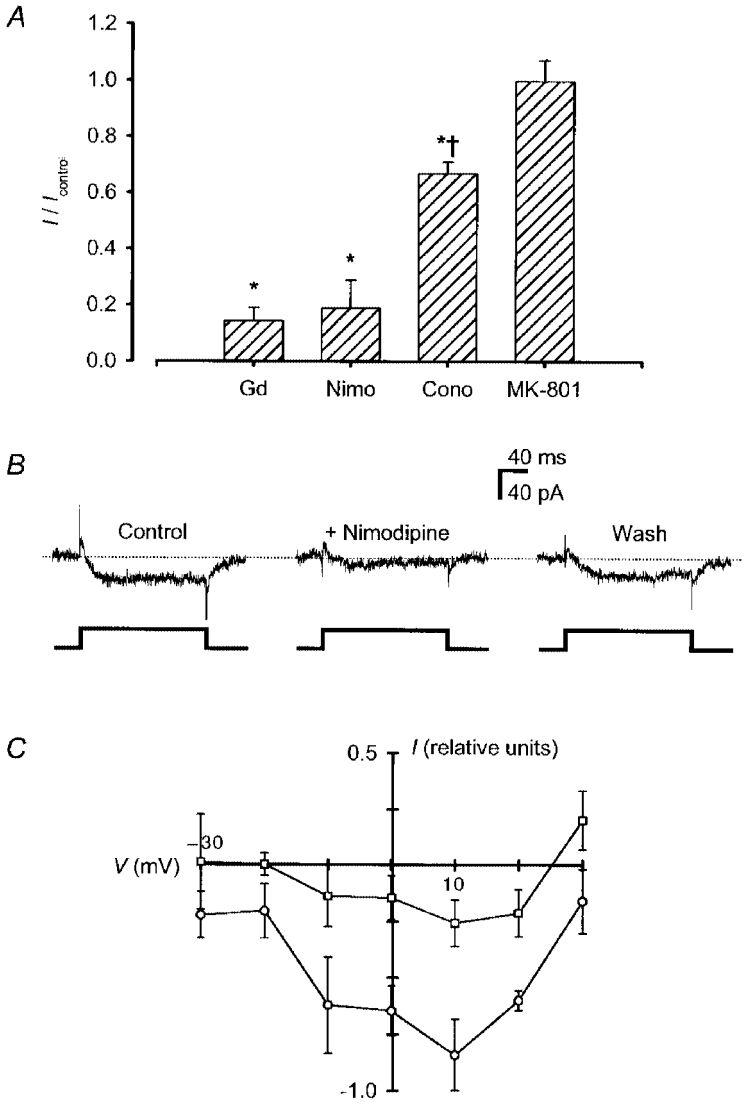

Figure 5. Zn^{2+} current was sensitive to blockade by non-specific and specific blockers of voltage-gated Ca^{2+} channels

A, steady-state Zn^{2+} current was inhibited by 10 μM Gd^{3+} (Gd), 1 μM nimodipine (Nimo), and 1 μM ω-conotoxin GVIA (Cono), but not by 1 μM MK-801. Zn^{2+} current was evoked by a voltage step to +10 mV in the presence of 2 mM Zn^{2+}. The level of steady-state current recorded in the presence of an antagonist was normalised to current amplitude measured with Zn^{2+} alone and plotted as the mean + S.E.M. of 3–8 cells per condition. Cells were perfused with drugs or control solution for 30 s between voltage step trials. * Significant difference between normalised steady-state current amplitudes measured in the presence and absence of an agent; † Significant difference compared to currents measured after treatment with nimodipine or Gd^{3+} ($P < 0{\cdot}05$, one-way ANOVA with Bonferroni's t test). *B*, current traces from a representative cell demonstrate reversible inhibition of Zn^{2+} current by 1 μM nimodipine; the cell was treated as in *A*. The dotted line represents the zero current level. *C*, the *I–V* relationship of steady-state currents recorded in the presence of 2 mM Zn^{2+} in the absence (○) or presence (□) of 1 μM nimodipine is plotted. *I–V* curves from 3 cells were normalised, each to its peak, and averaged. Points represent means ± S.E.M.

carried by 1 mM Ca^{2+} or 500 μM Zn^{2+}. In these experiments, intracellular pH was buffered to 7·4 with 10 mM Hepes (Table 1). Consistent with previous studies, lowering pH_o from 7·4 to 6·4 reversibly decreased Ca^{2+} current amplitude at 0 mV by 29 ± 2% ($n = 7$). In contrast, the same drop in pH_o reversibly enhanced Zn^{2+} current amplitude at 0 mV by 92 ± 10% ($n = 5$; Fig. 8*A*), and raising pH_o from 7·4 to 8·4 resulted in near-complete suppression of the Zn^{2+} current. Extracellular pH affected Zn^{2+} current in a graded fashion with an approximate pK of 7·4 (Fig. 8*C*). Compared to currents at pH_o 7·4, Zn^{2+} currents recorded at pH_o 6·4 were similarly sensitive to blockade by 10 μM Gd^{3+} (currents were suppressed by 86 ± 5%; $n = 4$; Fig. 8*B*) and had a similar time constant of Zn^{2+} current activation (Table 2).

We examined the effects of varying pH_o on the *I–V* relationship of the Zn^{2+} current. A decrease in pH_o was accompanied by an increase in inward steady-state Zn^{2+}

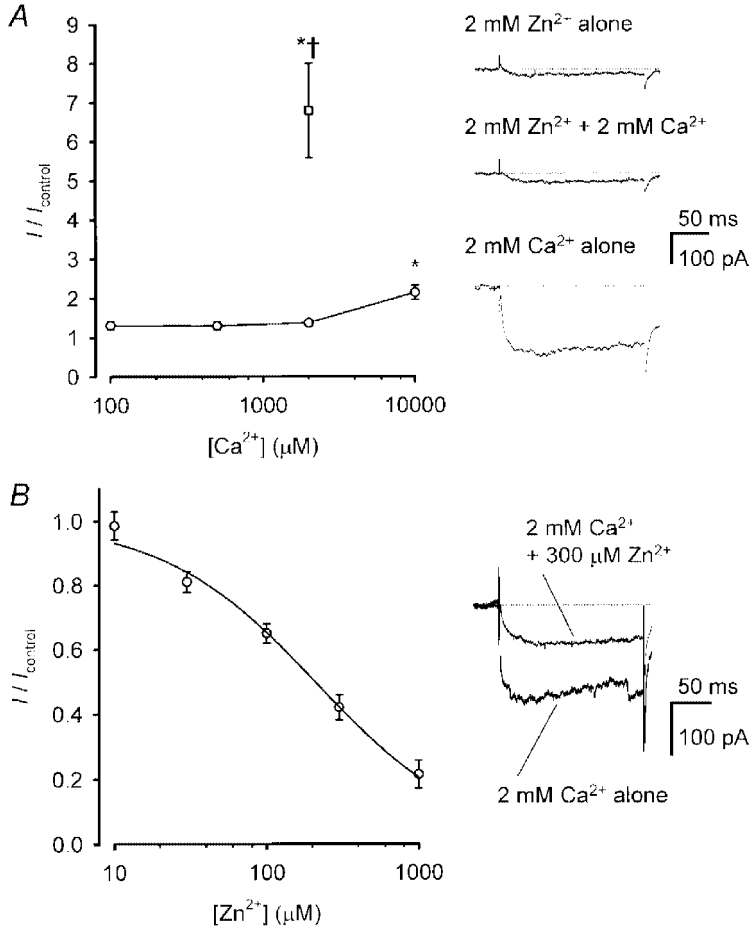

Figure 6. Zn^{2+} competed with Ca^{2+} for voltage-gated Ca^{2+} channel permeation

A, inward currents, evoked by voltage steps from −70 to +10 mV, were recorded from cells in the presence of 2 mM Zn^{2+} plus varying concentrations of Ca^{2+} (○; $n = 7$–14 cells per condition). Steady-state current amplitude is plotted relative to control currents evoked in the presence of 2 mM Zn^{2+} alone (left). Relative current amplitude recorded in the presence of 2 mM Ca^{2+} and no Zn^{2+} is plotted for comparison (□; $n = 4$). Points represent means ± S.E.M. Representative traces (right) show currents recorded in the presence of 2 mM Zn^{2+} with or without 2 mM Ca^{2+}; a representative trace from another neurone in the same culture dish, recorded in the presence of 2 mM Ca^{2+} alone, is illustrated for comparison. Dotted lines indicate the zero current level. * Significant difference between current amplitude in the indicated condition and control currents evoked in the presence of Zn^{2+} alone; † significant difference in current amplitudes recorded in the presence of 2 mM Ca^{2+} with *versus* without 2 mM Zn^{2+} ($P < 0{\cdot}05$, one-way ANOVA with Bonferroni's t test). *B*, inward currents, evoked by voltage steps from −70 to 0 mV, were recorded from 4 cells in the presence of 2 mM Ca^{2+} plus varying concentrations of Zn^{2+}. Steady-state current amplitude is plotted relative to currents evoked in the presence of 2 mM Ca^{2+} alone (left). Points represent means ± S.E.M. The points were fitted by a curve described by the equation:

$$I/I_{\text{control}} = \{1 + 10^{[\log(IC_{50}/Zn)/m]}\}^{-1},$$

where $IC_{50} = 210$ μM and $m = -1{\cdot}2$. Superimposed traces from a representative cell illustrate the effects of 300 μM Zn^{2+} on current recorded in the presence of 2 mM Ca^{2+} (right).

current amplitude at all membrane potentials as well as a positive shift in reversal potential ($n = 12$; Fig. 9*A*) from 29 mV at pH_o 7·4 to 59 mV at pH_o 6·4 (approximated by fitting curves to the *I–V* data; see Methods), although the voltage dependence of the estimated steady-state Zn^{2+} current activation was similar in both conditions, with V_h being −13 mV at pH_o 7·4 and −11 mV at pH_o 6·4 (Fig. 9*B*). These data suggest that the enhanced Zn^{2+} current observed at the lower pH_o was not due to an increase in the activity of free Zn^{2+} available for voltage-gated Ca^{2+} channel permeation, as an increase in $[Zn^{2+}]_o$ sufficient to double peak inward current would be expected to cause a considerable shift in V_h (see Fig. 4). Consistent with the hypothesis that the observed relationship between Zn^{2+} current amplitude

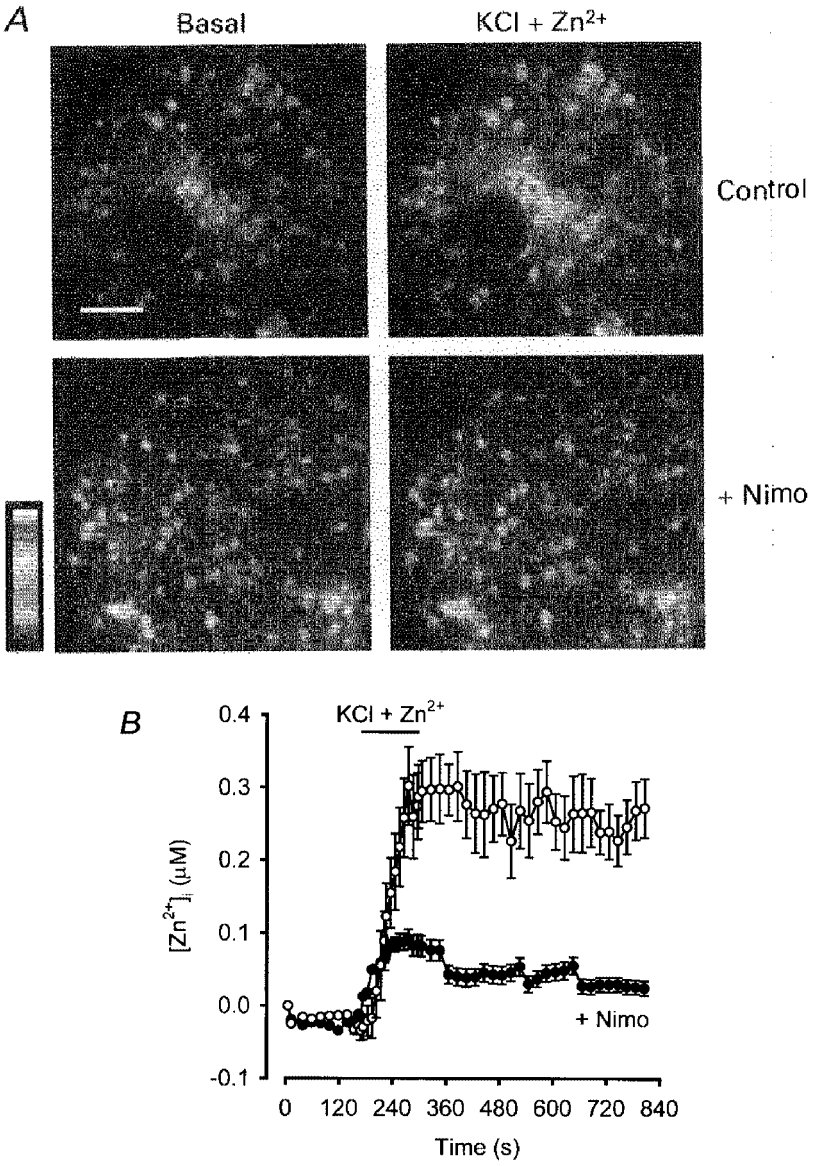

Figure 7. Voltage-gated Ca^{2+} channels mediated depolarisation-induced rises in $[Zn^{2+}]_i$ in physiological saline

A, cortical neuronal cultures loaded with Newport Green and bathed in Hepes-buffered saline (see Methods) were exposed for 2 min to either high-potassium + 300 μM Zn^{2+} (control) or high-potassium + 300 μM Zn^{2+} + 10 μM nimodipine (high-potassium solutions contained 60 mM KCl, 65 mM NaCl, and were otherwise identical to the Hepes-buffered saline). MK-801 (10 μM) and NBQX (10 μM) were present throughout experiments to block glutamate receptor activation by endogenous glutamate release. Pseudo-colour images from a representative experiment depict changes in $[Zn^{2+}]_i$ according to the Newport Green fluorescence values indicated in the scale. The fluorescence signal attributed to increased $[Zn^{2+}]_i$ was completely quenched by the addition of the selective membrane-permeable Zn^{2+} chelator, 100 μM TPEN (not shown). Scale bar = 50 μm. *B*, each trace represents the change in $[Zn^{2+}]_i$ observed in the same experiments described in *A* (control, $n = 57$ cells; nimodipine (Nimo), $n = 52$). Fluorescence values were converted to Zn^{2+} concentrations by a calibration performed at the end of the experiment (see Methods).

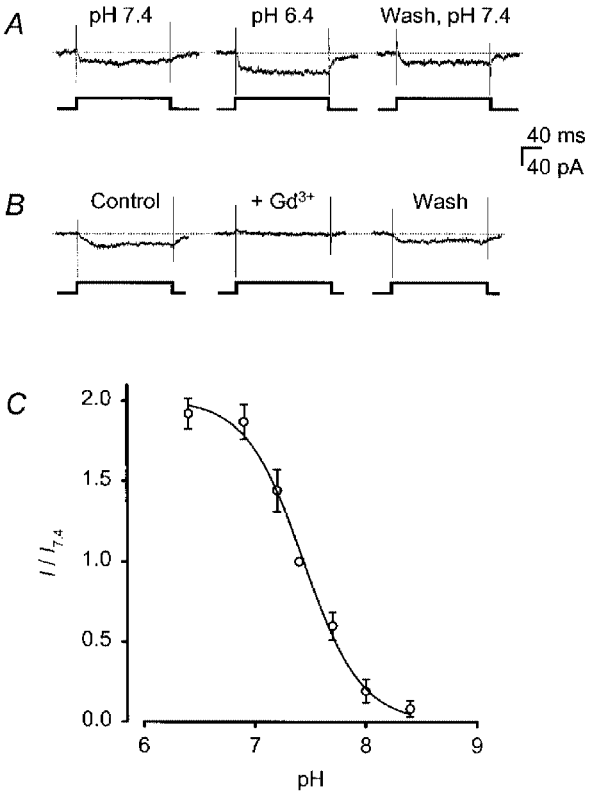

Figure 8. Extracellular acidity enhanced Zn^{2+} current

A, representative traces elicited by a voltage step to 0 mV in the presence of 500 μM Zn^{2+} show reversible changes in steady-state current amplitude at pH_o 6·4 compared to pH_o 7·4. Cells were exposed to a new extracellular buffer solution for 30–60 s between trials. This change in pH_o resulted in no change in the linearity of membrane currents throughout the range of voltages used by the leak subtraction protocol (see Methods; data not shown). *B*, representative traces recorded as in *A* at pH_o 6·4 show reversible blockade by 10 μM Gd^{3+}. *C*, steady-state Zn^{2+} current amplitudes at various test pH_o values are plotted relative to control currents at pH_o 7·4. Voltage steps to 0 mV were delivered to cells in the presence of 500 μM Zn^{2+}; a cell was perfused with a new extracellular buffer solution for 30–60 s between trials. Points represent means ± S.E.M. of 3–6 cells per condition and were fitted with a curve described by the equation:

$$(I/I_{7\cdot4}) = (I/I_{7\cdot4})_{max}[1 + 10^{(pK - pH)/m}]^{-1},$$

where $(I/I_{7\cdot4})_{max} = 2\cdot0$, $pK = 7\cdot4$, and $m = -1\cdot7$.

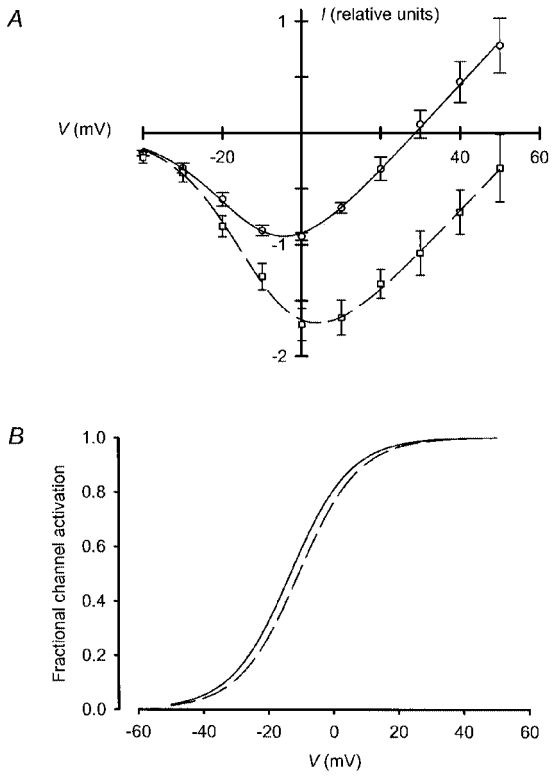

Figure 9. Extracellular acidity enhanced Zn^{2+} current amplitude with no effect on voltage sensitivity

A, the *I–V* relationships of currents recorded in the presence of 500 μM Zn^{2+} at pH_o 7·4 (○—○) and pH_o 6·4 (□– –□) were plotted. Twelve cells were tested, each at both pH_o values, and *I–V* curves for each cell were normalised to the peak inward steady-state current at pH_o 7·4. Points represent means ± S.E.M., and curves were fitted as in Fig. 4. At pH_o 7·4, $V_h = -13$ mV, $m = 9\cdot2$, $V_{rev} = 29$ mV, and $g = 0\cdot038$; at pH_o 6·4, $V_h = -11$ mV, $m = 9\cdot3$, $V_{rev} = 59$ mV, and $g = 0\cdot037$. *B*, decreasing pH_o from 7·4 (continuous line) to 6·4 (dashed line) resulted in little to no shift of the voltage sensitivity of channel activation. Curves were plotted as in Fig. 4.

and pH_o was not explained by changes in Zn^{2+} activity, the amount of zinc recoverable from solutions, which were prepared in the same plastic containers used in experiments and exposed to cultured cortical neurones, was no different at pH 6·4 than at 7·4 (Table 3).

Table 3. Atomic emission spectroscopic analysis of zinc recovered from experimental recording solutions in various conditions

Nominal $[Zn^{2+}]$ (μM)	pH	Exposure to cultures	Zinc recovered (p.p.m.)
500	7·4	−	28·8
500	6·4	−	29·5
0	7·4	−	< 0·5
0	6·4	−	< 0·5
500	7·4	+	28·0
500	6·4	+	29·1
0	7·4	+	< 0·5
0	6·4	+	< 0·5

Extracellular recording solutions (Table 1) were prepared at the indicated pH and $[Zn^{2+}]$ and stored in the same polypropylene containers used to store solutions during electrophysiological experiments. Some solutions were washed through cortical neuronal cultures before storage.

DISCUSSION

We demonstrate here that extracellular Zn^{2+} carried a voltage-activated inward current in murine cortical neurones exhibiting properties consistent with mediation by HVA Ca^{2+} channels. Under the recording conditions utilised, only extracellular Zn^{2+} or intracellular Cl^- were available to carry inward current, and current amplitude increased with increasing extracellular $ZnCl_2$. Consistent with the propensity of divalent cations to screen negative membrane surface charges (Hille, 1992), increasing $[Zn^{2+}]_o$ increased the threshold and peak potentials of the current's *I–V* relationship to a degree consistent with similar observations of Zn^{2+} currents in *Helix* neurones (Oyama *et al.* 1982). Relative to Ca^{2+} currents in these neurones, Zn^{2+} current was smaller and showed slower activation kinetics, and unlike Ca^{2+} currents, Zn^{2+} current did not exhibit voltage-dependent steady-state inactivation. In addition, Zn^{2+} was able to permeate voltage-gated Ca^{2+} channels in the presence of Ca^{2+}. Unexpectedly, Zn^{2+} current amplitude increased with decreasing pH_o, whereas HVA Ca^{2+} currents were suppressed by the same manoeuvre. Zn^{2+} current enhancement at lower pH_o was not accompanied by changes in activation kinetics or in the voltage sensitivity of channel gating.

Zn^{2+} current was mediated by voltage-gated Ca^{2+} channels

Supporting a role for HVA Ca^{2+} channels in mediating voltage-activated Zn^{2+} current, the *I–V* relationship of the current exhibited a profile typical for these channels (Fig. 1), and the current was sensitive to L- and N-type voltage-gated Ca^{2+} channel blockers (Figs 5 and 7). Nimodipine blocked a majority of Zn^{2+} entry into cortical neurones as measured both by electrophysiology and fluorescent dye imaging, suggesting that L-type channels carry the bulk of voltage-activated Zn^{2+} influx. ω-Conotoxin GVIA blocked a smaller proportion of the current, suggesting a smaller role for N-type channels. These data do not permit a calculation of the relative permeabilities of L- *versus* N-type channels to Zn^{2+}, as the magnitude of the pharmacological effects is also affected by differences in the population sizes and membrane distribution of these channel subtypes.

As noted above, previous electrophysiological studies of the effects of Zn^{2+} on mammalian voltage-gated Ca^{2+} channels have focused on the ability of Zn^{2+} to serve as a channel blocker (Winegar & Lansman, 1990; Büsselberg *et al.* 1992). However, Zn^{2+} permeation and blockade of current carried by other ions through voltage-gated Ca^{2+} channels may occur simultaneously, as has been proposed, for instance, in the interactions of Mg^{2+} (Ascher & Nowak, 1988) and Zn^{2+} (Christine & Choi, 1990) with NMDA receptor-gated channels. Winegar & Lansman (1990) showed that Zn^{2+} antagonises Ba^{2+} currents through single dihydropyridine-sensitive Ca^{2+} channels in mouse myotubes in a voltage-dependent manner, suggesting that Zn^{2+} binds in or near the channel pore. This blockade was characterised by an increase in open channel noise, presumably reflecting fast, unresolved blocking and unblocking of the channel, and calculations based on the kinetics of the blockade suggested that Zn^{2+} binds to open channels and has an exit rate from the pore faster than that of Mg^{2+}, Cd^{2+}, or La^{3+}. In addition, although the entry rate of Zn^{2+} into the Ca^{2+} channel pore was linearly dependent on $[Zn^{2+}]_o$, the exit rate was independent of Zn^{2+} concentration, suggesting, in agreement with data in the present study, that as Zn^{2+} exits a Ca^{2+} channel pore, it leaves from the cytoplasmic face.

Extracellular acidity enhanced Zn^{2+} current

In this study, decreasing pH_o was found to have opposite effects on inward currents carried by 500 μM Zn^{2+} and by 1 mM Ca^{2+}. The enhancement of Zn^{2+} current observed at acidic pH was not accompanied by a shift in the voltage sensitivity of the current (Fig. 9), as was seen when $[Zn^{2+}]_o$ was increased (Fig. 4), arguing against the possibility that this enhancement was due to an increase in free Zn^{2+}. In agreement with that observation, the amount of zinc recoverable from recording solutions was not affected by pH (Table 3).

The ability of decreasing pH_o to suppress HVA Ca^{2+} channel currents carried by Ca^{2+}, Ba^{2+}, or monovalent cations is well established, and appears to reflect some combination of two underlying mechanisms. First, experiments on single dihydropyridine-sensitive voltage-gated Ca^{2+} channels have suggested the existence of a low-conductance state for L-type

channels that is stabilised by protonation and destabilised by the binding of permeant cations (Prod'hom *et al.* 1987; Pietrobon *et al.* 1988). Second, H^+ may screen negative surface charges and thus alter the voltage dependence of channel gating (e.g. Iijima *et al.* 1986; Prod'hom *et al.* 1989).

Additional studies will be needed to delineate the mechanisms responsible for the paradoxical effect of lowering pH_o to enhance Zn^{2+} current through HVA Ca^{2+} channels. Perhaps H^+ permeates voltage-gated Ca^{2+} channels, and increased Zn^{2+} permeation does not account for the increased current amplitude. Arguing against this possibility is the observation that in the presence of monovalent cations as charge carriers, H^+ affects single L-type Ca^{2+} channels without apparently interacting with the channel pore (Prod'hom *et al.* 1987). Some controversy surrounds this point, as recent work has shown that the sensitivity of L-type Ca^{2+} channels to pH_o can be altered by mutagenesis of the glutamate residues that form the high-affinity Ca^{2+} interaction site in the channel pore (Chen *et al.* 1996), suggesting that pore interactions may indeed account for the ability of H^+ to elicit changes in channel conductance. However, single channel studies have revealed no direct competition between permeant cations and H^+ for entry into the channel (Pietrobon *et al.* 1988; Prod'hom *et al.* 1989); even if such competition were possible, Zn^{2+}, with a relatively high affinity for voltage-gated Ca^{2+} channel pore binding sites, might be expected to exclude H^+ from the pore even more effectively than other permeant cations.

Alternatively, extracellular H^+ may allosterically influence the permeability of voltage-gated Ca^{2+} channels (Prod'hom *et al.* 1987, 1989; Pietrobon *et al.* 1988, 1989), as is the case, for instance, for NMDA receptor-gated channels (Tang *et al.* 1990; Traynelis & Cull-Candy, 1990). A H^+-induced conformational change in voltage-gated Ca^{2+} channels may increase their permeability to Zn^{2+} while decreasing their permeability to Ca^{2+} and monovalent cations. The increase in reversal potential observed in Zn^{2+} currents at lower pH_o is consistent with an increase in permeability to Zn^{2+} relative to permeant intracellular cations, which, in these experiments, may include Na^+ or Li^+ (see Fig. 1 legend and Table 1). The fact that the net membrane conductance g (sum of all conductances when multiple permeant ions are present; see Methods), as estimated from curve fits to I–V data (Fig. 9*A*), did not change with a change in pH_o is consistent with a simple model in which a small absolute increase in Zn^{2+} conductance is counterbalanced by a comparable decrease in absolute conductance to permeant intracellular cations, although other scenarios cannot be excluded. Regardless of the exact underlying mechanism, the observed ability of extracellular acidity to enhance voltage-gated Ca^{2+} channel permeability to Zn^{2+} suggests that H^+ may have more complex effects on ion permeation through voltage-gated Ca^{2+} channels than previously thought.

Physiological significance

Both electrophysiological and fluorimetric evidence is presented supporting the notion that Zn^{2+} can permeate voltage-gated Ca^{2+} channels in the presence of physiological amounts of other cations, including Ca^{2+}. First, unlike the effect of Ca^{2+} on voltage-gated Ca^{2+} channel-mediated Ba^{2+} currents (Hille, 1992), no blockade of Zn^{2+} current was evident at low $[Ca^{2+}]_o$; net inward current amplitude in the presence of 2 mM extracellular Zn^{2+} was unaffected by up to equimolar amounts of extracellular Ca^{2+}. When $[Ca^{2+}]_o$ exceeded $[Zn^{2+}]_o$, at least some of the inward current was probably carried by Ca^{2+}, but the presence of Zn^{2+} clearly impeded voltage-gated Ca^{2+} channel permeability to Ca^{2+}. As in other cell types, Zn^{2+} blocked cortical neuronal voltage-gated Ca^{2+} currents. Second, neurones loaded with the fluorescent Zn^{2+} probe Newport Green exhibited depolarisation-evoked increases in $[Zn^{2+}]_i$ in the presence of physiological concentrations of extracellular cations plus 300 μM extracellular Zn^{2+}. Depolarisation-evoked Zn^{2+} influx was largely inhibited by nimodipine, implicating L-type Ca^{2+} channels as the major mediators of membrane permeability to Zn^{2+}. In these experiments, $[Ca^{2+}]_o$ exceeded $[Zn^{2+}]_o$ by sixfold.

The demonstration that murine neuronal voltage-gated Ca^{2+} channels can carry an inward Zn^{2+} current supports the notion that blockade of these channels may have therapeutic utility in pathological conditions, such as cardiac arrest or sustained seizures, where excessive Zn^{2+} influx may contribute to neuronal death (Choi & Koh, 1998). Although the absolute permeability of voltage-gated Ca^{2+} channels to Zn^{2+} is low compared to Ca^{2+}, these channels exhibited much less voltage-dependent steady-state inactivation when Zn^{2+}, instead of Ca^{2+}, was used as the charge carrier (Fig. 2). These data suggest that voltage-gated Ca^{2+} channels could indeed mediate the sustained increases in $[Zn^{2+}]_i$ observed in conditions where Zn^{2+} is toxic to cortical neurones (Canzoniero *et al.* 1999). In addition, data presented here raise the novel possibility that the neurotoxic contribution of Zn^{2+} influx through HVA Ca^{2+} channels may be specifically enhanced by increases in extracellular acidity caused by the build-up of brain lactate associated with ischaemic conditions.

Aballay, A., Sarrouf, M. N., Colombo, M. I., Stahl, P. D. & Mayorga, L. S. (1995). Zn^{2+} depletion blocks endosome fusion. *Biochemical Journal* **312**, 919–923.

Almers, W. & McCleskey, E. W. (1984). Non-selective conductance in calcium channels of frog muscle: calcium selectivity in a single-file pore. *Journal of Physiology* **353**, 585–608.

Ascher, P. & Nowak, L. (1988). The role of divalent cations in the *N*-methyl-D-aspartate responses of mouse central neurones in culture. *Journal of Physiology* **399**, 247–266.

Assaf, S. Y. & Chung, S. H. (1984). Release of endogenous Zn^{2+} from brain tissue during activity. *Nature* **308**, 734–736.

Atar, D., Backx, P. H., Appel, M. M., Gao, W. D. & Marban, E. (1995). Excitation-transcription coupling mediated by zinc influx through voltage-dependent calcium channels. *Journal of Biological Chemistry* **270**, 2473–2477.

Büsselberg, D., Michael, D., Evans, M. L., Carpenter, D. O. & Haas, H. L. (1992). Zinc (Zn^{2+}) blocks voltage gated calcium channels in cultured rat dorsal root ganglion cells. *Brain Research* **593**, 77–81.

Canzoniero, L. M., Taglialatela, M., Di Renzo, G. & Annunziato, L. (1993). Gadolinium and neomycin block voltage-sensitive Ca^{2+} channels without interfering with the Na^{+}-Ca^{2+} antiporter in brain nerve endings. *European Journal of Pharmacology* **245**, 97–103.

Canzoniero, L. M. T., Turetsky, D. M. & Choi, D. W. (1999). Measurement of intracellular free zinc concentrations accompanying zinc-induced neuronal death. *Journal of Neuroscience* **19**, RC31: 1–6.

Chen, X.-H., Bezprozvanny, I. & Tsien, R. W. (1996). Molecular basis of proton block of L-type Ca^{2+} channels. *Journal of General Physiology* **108**, 363–374.

Choi, D. W. & Koh, J. Y. (1998). Zinc and brain injury. *Annual Review of Neuroscience* **21**, 347–375.

Choi, D. W., Yokoyama, M. & Koh, J. (1988). Zinc neurotoxicity in cortical cell culture. *Neuroscience* **24**, 67–79.

Christine, C. W. & Choi, D. W. (1990). Effect of zinc on NMDA receptor-mediated channel currents in cortical neurons. *Journal of Neuroscience* **10**, 108–116.

Frederickson, C. J. (1989). Neurobiology of zinc and zinc-containing neurons. *International Review of Neurobiology* **31**, 145–238.

Freund, W.-D. & Reddig, S. (1994). AMPA/Zn^{2+}-induced neurotoxicity in rat primary cortical cultures: involvement of L-type calcium channels. *Brain Research* **654**, 257–264.

Fukuda, J. & Kawa, K. (1977). Permeation of manganese, cadmium, zinc, and beryllium through calcium channels of an insect muscle membrane. *Science* **196**, 309–311.

Grynkiewicz, G., Poenie, M. & Tsien, R. Y. (1985). A new generation of Ca^{2+} indicators with greatly improved fluorescence properties. *Journal of Biological Chemistry* **260**, 3440–3450.

Hagiwara, S. & Takahashi, K. (1967). Surface density of calcium ions and calcium spikes in the barnacle muscle fiber membrane. *Journal of General Physiology* **50**, 583–601.

Harrison, N. L. & Gibbons, S. J. (1994). Zn^{2+}: an endogenous modulator of ligand- and voltage-gated ion channels. *Neuropharmacology* **33**, 935–952.

Haugland, R. P. (1996). *Handbook of Fluorescent Probes and Research Chemicals*, 6th edn, ed. Spence, M. T. Z., pp. 531–540. Molecular Probes, Eugene, OR, USA.

Hille, B. (1992). *Ionic Channels of Excitable Membranes*. Sinauer Associates Inc., MA, USA.

Howell, G. A., Welch, M. G. & Frederickson, C. J. (1984). Stimulation-induced uptake and release of zinc in hippocampal slices. *Nature* **308**, 736–738.

Iijima, T., Ciani, S. & Hagiwara, S. (1986). Effects of the external pH on Ca channels: experimental studies and theoretical considerations using a two-site, two-ion model. *Proceedings of the National Academy of Sciences of the USA* **83**, 654–658.

Kawa, K. (1979). Zinc-dependent action potentials in giant neurons of the snail, *Euhadra quaestia*. *Journal of Membrane Biology* **49**, 325–344.

Kerchner, G. A., Yu, S. P. & Choi, D. W. (1998). Measurement of zinc current through cortical neuronal voltage-gated calcium channels: enhancement by extracellular acidity. *Society for Neuroscience Abstracts* **24**, 466.

Koh, J.-Y. & Choi, D. W. (1994). Zinc toxicity on cultured cortical neurons: involvement of N-methyl-D-aspartate receptors. *Neuroscience* **60**, 1049–1057.

Koh, J.-Y., Suh, S. W., Gwag, B. J., He, Y. Y., Hsu, C. Y. & Choi, D. W. (1996). The role of zinc in selective neuronal death after transient global cerebral ischemia. *Science* **272**, 1013–1016.

Kostyuk, P. G., Mironov, S. L. & Shuba, Ya. M. (1983). Two ion-selecting filters in the calcium channel of the somatic membrane of mollusc neurons. *Journal of Membrane Biology* **76**, 83–93.

Lansman, J. B. (1990). Blockade of current through single calcium channels by trivalent lanthanide cations: effect of ionic radius on the rates of ion entry and exit. *Journal of General Physiology* **95**, 679–696.

Lobner, D., Canzoniero, L. M. T., Manzerra, P., Gottron, F., Ying, H., Knudson, M., Tian, M., Dugan, L. L., Kerchner G. A., Sheline, C. T., Korsmeyer, S. J. & Choi, D. W. (2000). Zinc-induced neuronal death in cortical neurons. *Cellular and Molecular Biology* **46**, 797–806.

Manev, H., Kharlamov, E., Uz, T., Mason, R. P. & Cagnoli, C. M. (1997). Characterization of zinc-induced neuronal death in primary cultures of rat cerebellar granule cells. *Experimental Neurology* **146**, 171–178.

Oyama, Y., Nishi, K., Yatani, A. & Akaike, N. (1982). Zinc current in *Helix* soma membrane. *Comparative Biochemistry and Physiology* **72C**, 403–410.

Perez-Clausell, J. & Danscher, G. (1985). Intravesicular localization of zinc in rat telencephalic boutons: a histochemical study. *Brain Research* **337**, 91–98.

Pietrobon, D., Prod'hom, B. & Hess, P. (1988). Conformational changes associated with ion permeation in L-type calcium channels. *Nature* **333**, 373–376.

Pietrobon, D., Prod'hom, B. & Hess, P. (1989). Interactions of protons with single open L-type calcium channels: pH dependence of proton-induced current fluctuations with Cs^{+}, K^{+}, and Na^{+} as permeant ions. *Journal of General Physiology* **94**, 1–21.

Prod'hom, B., Pietrobon, D. & Hess, P. (1987). Direct measurement of proton transfer rates to a group controlling the dihydropyridine-sensitive Ca^{2+} channel. *Nature* **329**, 243–246.

Prod'hom, B., Pietrobon, D. & Hess, P. (1989). Interactions of protons with single open L-type calcium channels: location of protonation site and dependence of proton-induced current fluctuations on concentration and species of permeant ion. *Journal of General Physiology* **94**, 23–42.

Rose, K., Goldberg, M. P. & Choi, D. W. (1993). Cytotoxicity in murine neocortical cell culture. In *Methods in Toxicology*, ed. Tyson, C. A. & Frazier, J. M., pp. 46–60. Academic Press, San Diego, CA, USA.

Sensi, S. L., Canzoniero, L. M. T., Yu, S. P., Ying, H. S., Koh, J.-Y., Kerchner, G. A. & Choi, D. W. (1997). Measurement of intracellular free zinc in living cortical neurons: routes of entry. *Journal of Neuroscience* **17**, 9554–9564.

Sensi, S. L., Yin, H. Z., Carriedo, S. G., Rao, S. S. & Weiss, J. H. (1999). Preferential Zn^{2+} influx through Ca^{2+}-permeable AMPA/kainate channels triggers prolonged mitochondrial superoxide production. *Proceedings of the National Academy of Sciences of the USA* **96**, 2414–2419.

Smart, T. G., Xie, X. & Krishek, B. J. (1994). Modulation of inhibitory and excitatory amino acid receptor ion channels by zinc. *Progress in Neurobiology* **42**, 393–441.

Tang, C. M., Dichter, M. & Morad, M. (1990). Modulation of the N-methyl-D-aspartate channel by extracellular H^+. *Proceedings of the National Academy of Sciences of the USA* **87**, 6445–6449.

Tombaugh, G. C. & Somjen, G. G. (1996). Effects of extracellular pH on voltage-gated Na^+, K^+, and Ca^{2+} currents in isolated rat CA1 neurons. *Journal of Physiology* **493**, 719–732.

Tønder, N., Johansen, F. F., Frederickson, C. J., Zimmer, J. & Diemer, N. H. (1990). Possible role of zinc in the selective degeneration of dentate hilar neurons after cerebral ischemia in the adult rat. *Neuroscience Letters* **109**, 247–252.

Traynelis, S. F. & Cull-Candy, S. G. (1990). Proton inhibition of N-methyl-D-aspartate receptors in cerebellar neurons. *Nature* **345**, 347–350.

Vega, M. T., Villalobos, C., Garrido, B., Gandía, L., Bulbena, O., García-Sancho, J., García, A. G. & Artalejo, A. R. (1994). Permeation by zinc of bovine chromaffin cell calcium channels: relevance to secretion. *Pflügers Archiv* **429**, 231–239.

Vogt, K., Mellor, J., Tong, G. & Nicoll, R. (2000). The actions of synaptically released zinc at hippocampal mossy fiber synapses. *Neuron* **26**, 187–196.

Weiss, J. H., Hartley, D. M., Koh, J.-Y. & Choi, D. W. (1993). AMPA receptor activation potentiates zinc neurotoxicity. *Neuron* **10**, 43–49.

Winegar, B. D. & Lansman, J. B. (1990). Voltage-dependent block by zinc of single calcium channels in mouse myotubes. *Journal of Physiology* **425**, 563–578.

Yin, H. Z. & Weiss, J. H. (1995). Zn^{2+} permeates Ca^{2+} permeable AMPA/kainate channels and triggers selective neural injury. *NeuroReport* **6**, 2553–2556.

Yokoyama, M., Koh, J. & Choi, D. W. (1986). Brief exposure to zinc is toxic to cortical neurons. *Neuroscience Letters* **71**, 351–355.

Acknowledgements

We wish to thank J. H. Steinbach and C. J. Lingle for their helpful comments on the manuscript. This work was supported in part by a Howard Hughes Medical Institute Medical Student Research Training Fellowship (G.A.K.) and NIH grant NS 32636 (D.W.C.).

Corresponding author

D. W. Choi: Department of Neurology, Washington University School of Medicine, Campus Box 8111, 660 S. Euclid Avenue, St Louis, MO 63110, USA.

Email: choid@neuro.wustl.edu